

Analysis of Inductively Injection Locked Oscillators at an Integer Frequency Ratio

Franco Ramírez¹, Robert Melville², Almudena Suárez¹

¹University of Cantabria, Spain

²Emecon, LLC, USA

ramirezf@unican.es, robert.melville@ieee.org, almudena.suarez@unican.es

Abstract — Oscillators under inductive resonant coupling are used to reduce phase noise in frequency generation and can also be applied to implement sensor systems. Here the operation of two inductively locked oscillators at an integer frequency ratio is analysed in depth, paying attention to the locking mechanism and identifying the various kinds of steady state solutions. The injection-locked solution curve versus the parameter used for control or sensing is obtained through harmonic balance with the aid of auxiliary generators. When increasing the coupling effects, the locked-operation interval undergoes a significant shift versus the parameter, which is understood with the aid of an analytical formulation. The stability properties and phase noise are analysed by linearizing the system about the mutually injection-locked steady-state solution, through the extraction of an outer-tier Jacobian matrix. The results are validated with time-domain maps based on maxima detection and with measurements.

Keywords — inductive coupling, oscillator, injection locking

I. INTRODUCTION

Several works propose the use of oscillators under inductive resonant coupling for phase-noise reduction in frequency generation [1]-[2]. In this application, the inductive coupling generally takes place between identical oscillators at the same frequency. On the other hand, configurations based on two coupled oscillators enable the implementation of differential sensors [3]. As shown in [4], in some applications, it is convenient to use oscillators at an integer frequency ratio 1: N , so that only one of the oscillators (at either ω or $N\omega$) is sensitive to the measurand. The locking at 1: N can also be useful to obtain concurrent harmonic oscillations, with application in harmonic radar schemes [5]. Despite their interest, the behaviour of inductively coupled oscillators is rather complex as shown in [6], which mainly focuses on the case of two oscillators operating at the same fundamental frequency.

The previous works [6]-[7] presented a preliminary study of inductively coupled oscillators at a ratio 1: N , which due to several simplifying assumptions, was limited to small values of the coupling factor. The study did not delve into the various kinds of system solutions and their evolution and qualitative changes as this factor increases. In implementations such as the one in [4], the coupling factor can be relatively strong, so there is a need for an accurate prediction of the behaviour in these conditions. This will be achieved here through harmonic-balance (HB) simulations based on the use of auxiliary generators (AGs) [8]-[9]. As will be demonstrated, the stability and phase noise analysis cannot be carried out linearizing the

system about the free-running solutions of the two oscillators, as done in previous works [6]-[8]. Instead, the system will be linearized, for the first time, about each mutually locked solution by extracting an outer-tier Jacobian matrix from HB.

The main contribution of the work is the derivation of new analysis methods, which have been tested in a system of two coupled oscillators at the ratio 1:3. The fundamental frequency is chosen low (10 MHz) to facilitate the validation with independent simulations based on time-domain integration. Because the methods are based on HB, they can be applied to circuits in the microwave range.

II. INDUCTIVELY COUPLED OSCILLATORS

We assume that in isolated conditions, the two coupled oscillators have the fundamental frequencies ω_{a0} and $\omega_{b0} \cong N\omega_{a0}$. In mutually injection-locked operation (Fig. 1), one will have $\omega_b = N\omega_a$. At the harmonic frequency $m\omega$, where m is an integer and $\omega = \omega_a$, the inductive coupling matrix is:

$$\begin{bmatrix} y_{11} & y_{12} \\ y_{21} & y_{22} \end{bmatrix} = \begin{bmatrix} \frac{-j}{(1-k^2)L_1m\omega} & \frac{jk}{(1-k^2)\sqrt{L_1L_2}m\omega} \\ \frac{jk}{(1-k^2)\sqrt{L_1L_2}m\omega} & \frac{-j}{(1-k^2)L_2m\omega} \end{bmatrix} \quad (1)$$

where k is the coupling factor. For simplicity, we will describe the two oscillators with their admittance functions defined from their connection ports to the coupling network (Fig. 1). At each m^{th} harmonic, one has the subsystem:

$$\begin{aligned} I_{T,a,m} &= \left[Y_{a,m}(m\omega, \bar{V}_a) - \frac{j}{(1-k^2)L_1m\omega} \right] V_{a,m} + \frac{jkV_{b,m}}{(1-k^2)\sqrt{L_1L_2}m\omega} = 0 \\ I_{T,b,m} &= \frac{jkV_{a,m}}{(1-k^2)\sqrt{L_1L_2}m\omega} + \left[Y_{b,m}(m\omega, \bar{V}_b) - \frac{j}{(1-k^2)L_2m\omega} \right] V_{b,m} = 0 \end{aligned} \quad (2)$$

where $m = 1$ to NH , $V_{a,m}$ and $V_{b,m}$ are the complex voltages at the ports of the two oscillators, $Y_{a,m}$ and $Y_{b,m}$ are the nonlinear admittance functions, each depending on all the harmonic terms of its corresponding set state variables, \bar{V}_a and \bar{V}_b , respectively, and $I_{T,a,m}$ and $I_{T,b,m}$ are the total currents. Though the two oscillators are mutually locked, the system is autonomous since the fundamental frequency ω is self-generated and, thus, an unknown of the problem. Because there is invariance with respect to the phase shift, one can arbitrarily set the phase of one state variable to zero. The two subcircuits must be in an oscillatory state at the respective frequencies ω and $N\omega$. Note

that in [6]-[7], the inductive coupling effects at frequencies different from $N\omega$ were disregarded.

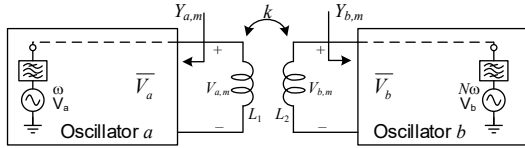


Fig. 1. Sketch of two oscillators described with admittance functions defined at the ports at which they are connected to the coupling network.

From a simple inspection of (2), under $k=0$, the two subcircuits are uncoupled and should oscillate at their standalone frequencies independently, at ω_{a0} and $\omega_{b0} \cong N\omega_{a0}$. As k increases, the solution in each oscillator will progressively deviate from the standalone one, and because $\omega_{b0} \cong N\omega_{a0}$ one can expect the existence of parameter interval in which (2) is fulfilled. A default HB simulation in commercial software provides only one of the two oscillations (at either ω or $N\omega$), depending on the location of the analysis ports or nodes. To enforce the mutually locked oscillatory state, we will use two AGs connected to the two sub-oscillators (Fig. 1). Calculating the ratio between each AG current and voltage, one obtains the following system of two complex equations in the four unknowns $|V_a|, \phi_{a,1}, |V_{b,N}|, \omega$:

$$Y_{T,a}(|V_{a,1}|, \phi_{a,1}, |V_{b,N}|, \omega) = \frac{I_{a,1}}{|V_{a,1}| e^{j\phi_{a,1}}} = 0 \quad (3)$$

$$Y_{T,b}(|V_{a,1}|, \phi_{a,1}, |V_{b,N}|, \omega) = \frac{I_{b,N}}{|V_{b,N}|} = 0$$

Note that the remaining equations (at all the rest of nodes and harmonic terms) act like an inner tier. Due to the autonomy of the system, in (3) we have arbitrarily set the phase origin at the AG at $N\omega$, in the higher-frequency oscillator (oscillator “b”). The solution curves are obtained by sweeping the phase ϕ of the lower-frequency AG and solving the system of two outer-tier equations in (3) at each sweep step. Due to the frequency ratio $1:N$, it is sufficient to sweep the phase $\phi_{a,1}$ between 0 and $2\pi/N$.

The method has been applied to analyze the system in Fig. 2, composed of two differential bipolar-based oscillators coupled at the ratio 1:3. When isolated from each other, the two circuits oscillate at the respective frequencies 10 MHz and 30 MHz. For the analysis based on (3), two AGs with the same amplitude and 180° phase shift are connected at equivalent nodes of each oscillator circuit to preserve the differential operation. However, due to the circuit symmetry, it suffices to impose conditions (3) to one AG in each oscillator. The family of solution curves versus the capacitor C_1 , obtained when increasing the coupling factor k , is shown in Fig. 3. The circuit behaves in mutually injection-locked operation in the closed curves. Fig. 3(a) presents the voltage amplitude at the collector node of the lower frequency oscillator (oscillator “a”) at the frequency ω . The locked solutions and those obtained when only the oscillator “a” is in an oscillatory state (open curves) can be seen. Note that there will be no signal at ω when only the higher-frequency oscillator “b” is in an oscillatory state. Fig. 3(b) presents the voltage amplitude at 3ω in the second

oscillator. Besides the locked solution curves, there are two families of open curves. The higher amplitude ones are obtained when only the oscillator “b” (at 3ω) is in an oscillatory state. The lower amplitude curves are obtained when only the oscillator “a” is in an oscillatory state and are basically due to the coupling of the third harmonic component of the oscillation in (a). These open solution curves are significant since they can become stable in certain parameter intervals, as shown later in this section. As gathered from Fig. 3(a) and (b), in locked conditions the amplitude in each oscillator is smaller than the one obtained when only this oscillator is in an oscillatory state, due to the reduction of negative conductance in the presence of a significant signal coupled from the other oscillator.

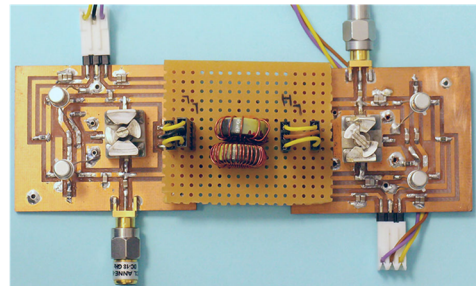
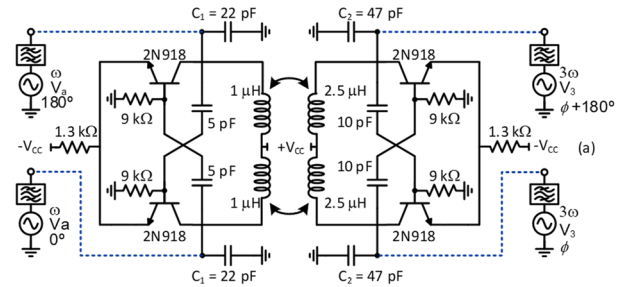


Fig. 2. Oscillator system based on two differential bipolar-based oscillators coupled at the ratio 1:3. (a) Schematic, showing the connection of the four AGs. (b) Photograph of the oscillators.

The locked-operation intervals predicted by the solution curves in Fig. 3 have been verified through time-domain integration plus a mapping technique. For each parameter value one obtains the steady-state waveform $v(t)$ and subtracts from it its average value v_o . Then, one detects the maxima in the window defined between each consecutive pair of zero crossings. These detections must be carried out for a sufficiently long-time interval in steady-state operation. The results are presented in Fig. 4. In sections with mutually locked operation at $\omega_b = 3\omega$ one obtains three maxima. In regions with quasi-periodic operation, one obtains a distribution of points. In fact, for low and intermediate k , outside the closed solution curves the circuit behaves in a double autonomous quasi-periodic regime, with two incommensurate fundamental frequencies, one delivered by each oscillator. Comparing Fig. 3(a) and (b) with Fig. 4(a) and (b) one notes that there is an excellent agreement in the prediction of the locked intervals. The apparent amplitude discrepancy is because the time domain simulations include the DC biasing.

The coupling factor in the circuit implementation, estimated through measurements, is $k=0.2$. Experimental points are shown in the inset. The open solution curve in which only “b”

oscillates becomes stable from certain k , as shown in the time-domain map of Fig. 4(c), which from $C_1 = 72$ pF only exhibits one point, corresponding a single peak in the solution waveform (a single oscillation, instead of two coherent ones at the ratio at the ratio 1:3). The frequency variation versus C_1 is shown in Fig. 3(c). Note the near linear variation in locked conditions in each capacitor interval, with similar sensitivity and a progressively larger tuning range in the successive locking windows. For a rough estimation of the shift in the C_1 intervals leading to locked operation, we can consider the equivalent self-inductance exhibited by the coupling network $(1-k^2)L_1$, in the higher frequency oscillator. Assuming an oscillation frequency close to its original value $f_{ao} = 10$ MHz and $\omega_{bo} \cong N\omega_{ao}$, the required C_1 shifts with k according to the relationship: $C_1 = [(1-k^2)L_2(3\omega_{ao})^2]^{-1}$. For instance, at $k=0.5$ (0.6), the above expression predicts a locking interval about $C_1 = 37$ pF (44 pF). The phase shift $\phi_{a,1}$, is shown in Fig. 3(d). The phase sensitivity to variations in C_1 decreases with k . However, under too small k the system will not be robust, so a compromise is needed. From Fig. 3, under inductive coupling, the locked operation can be achieved for a large interval of capacitor values by simply adjusting k , which enables design versatility. Note that the purpose here is to provide general analysis tools, instead of optimizing the system for a particular application.

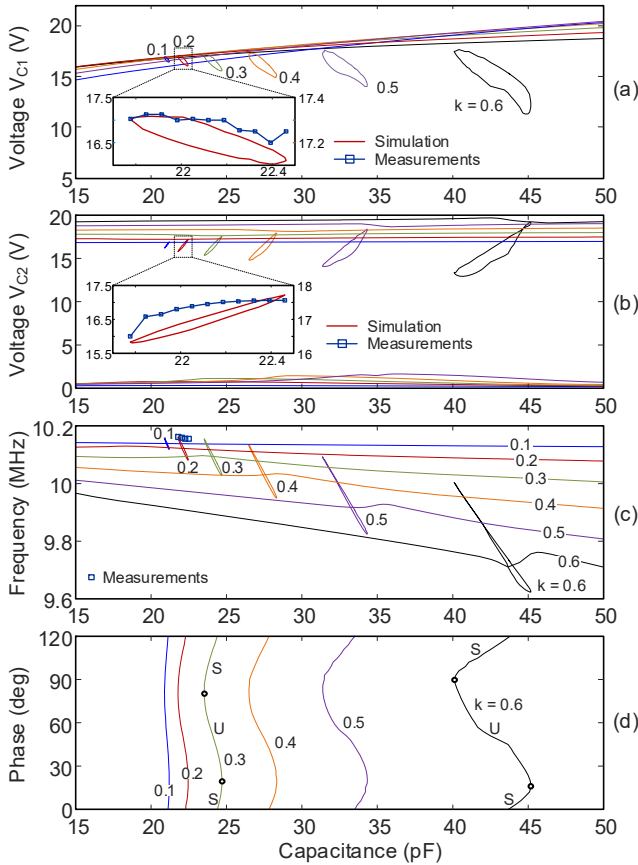


Fig. 3. Family of solution curves in of the system of two inductively coupled oscillators obtained through HB simulations with the aid of four AGs. Measurements are also shown. (a) Amplitude at the higher-frequency oscillator. (b) Amplitude at the lower frequency oscillator. (c) Oscillation frequency. (d) Phase shift. S, stable; U, unstable.

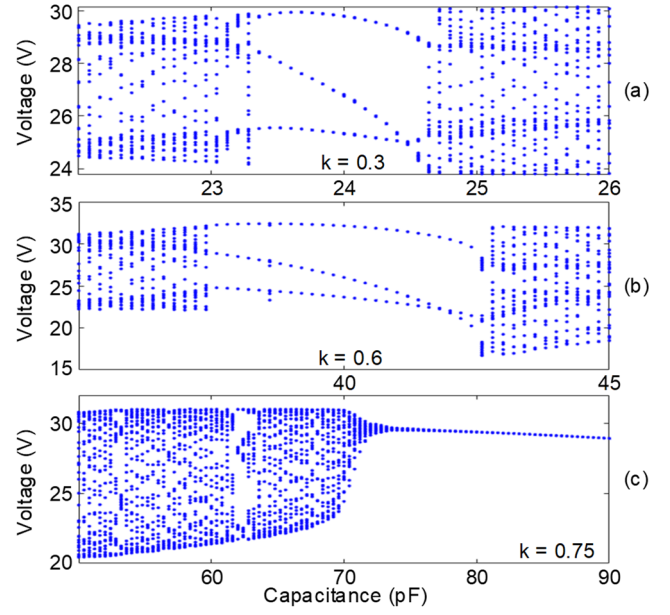


Fig. 4. Validation of the family of solution curves in Fig. 3 through time-domain integration and a mapping technique. (a) $k = 0.3$. (b) $k = 0.6$. (c) $k = 0.75$.

III. STABILITY AND PHASE NOISE ANALYSIS

For the stability and phase noise analysis, we will introduce a small perturbation in system (3) and linearize the outer-tier system about each mutually locked solution. This is different from previous approaches [7]–[8], in which this linearization was carried out about the free-running solutions of the uncoupled oscillators. Such a linearization becomes invalid even from relatively small k , due to the significant shift versus the parameter of the solution curves demonstrated here. Expressing the complex frequency increments as $\delta|\dot{V}_{a,1}|/|V_{a,1}| + \delta\dot{\phi}_{a,1}$, $\delta|\dot{V}_{b,N}|/|V_{b,N}| + \delta\dot{\phi}_{b,N}$ [8], one obtains:

$$\frac{\partial I_{a,1}^r}{\partial \omega} \frac{\delta|\dot{V}_{a,1}|}{|V_{a,1}|} + \frac{\partial I_{a,1}^r}{\partial \omega} \delta\dot{\phi}_{a,1} = \frac{\partial I_{a,1}^r}{\partial |V_{a,1}|} \delta|V_{a,1}| + \frac{\partial I_{a,1}^r}{\partial |V_{b,N}|} \delta|V_{b,N}| \frac{\partial I_{a,1}^r}{\partial \phi_{a,1}} \delta\phi_{a,1} - \frac{\partial I_{a,1}^r}{\partial \phi_{b,N}} \delta\phi_{b,N} \quad (4)$$

$$\frac{\partial I_{a,1}^i}{\partial \omega} \frac{\delta|\dot{V}_{a,1}|}{|V_{a,1}|} + \frac{\partial I_{a,1}^i}{\partial \omega} \delta\dot{\phi}_{a,1} = \frac{\partial I_{a,1}^i}{\partial |V_{a,1}|} \delta|V_{a,1}| + \frac{\partial I_{a,1}^i}{\partial |V_{b,N}|} \delta|V_{b,N}| \frac{\partial I_{a,1}^i}{\partial \phi_{a,1}} \delta\phi_{a,1} - \frac{\partial I_{a,1}^i}{\partial \phi_{b,N}} \delta\phi_{b,N} \quad (5)$$

$$\frac{\partial I_{b,N}^i}{\partial \omega} \frac{\delta|\dot{V}_{b,N}|}{|V_{b,N}|} + \frac{\partial I_{b,N}^i}{\partial \omega} \delta\dot{\phi}_{b,N} = \frac{\partial I_{b,N}^i}{\partial |V_{a,1}|} \delta|V_{a,1}| + \frac{\partial I_{b,N}^i}{\partial |V_{b,N}|} \delta|V_{b,N}| \frac{\partial I_{b,N}^i}{\partial \phi_{a,1}} \delta\phi_{a,1} - \frac{\partial I_{b,N}^i}{\partial \phi_{b,N}} \delta\phi_{b,N} \quad (6)$$

$$\frac{\partial I_{b,N}^r}{\partial \omega} \frac{\delta|\dot{V}_{b,N}|}{|V_{b,N}|} + \frac{\partial I_{b,N}^r}{\partial \omega} \delta\dot{\phi}_{b,N} = \frac{\partial I_{b,N}^r}{\partial |V_{a,1}|} \delta|V_{a,1}| + \frac{\partial I_{b,N}^r}{\partial |V_{b,N}|} \delta|V_{b,N}| \frac{\partial I_{b,N}^r}{\partial \phi_{a,1}} \delta\phi_{a,1} - \frac{\partial I_{b,N}^r}{\partial \phi_{b,N}} \delta\phi_{b,N} \quad (7)$$

where the current derivatives are calculated applying finite differences to the AGs used to obtain the steady-state solution. Defining the vector $\delta\bar{X} = [\delta|V_{a,1}| \ \delta|V_{b,N}| \ \delta\phi_{a,1} \ \delta\phi_{b,N}]^T$ one can express: $\delta\bar{X} = [M]\delta\bar{X}$, so the stability properties are given by the eigenvalues of M . In Fig. 5 the real parts of these eigenvalues have been traced versus the phase shift for two k values. Note that one of these eigenvalues is always zero due to the solution autonomy. For $k = 0.3$, only the three larger real eigenvalues are represented. In the two cases, at the limits of the stable phase shift interval a real eigenvalue crosses through zero, which occurs at each of the two turning points of the closed solution curve versus C_1 [Fig. 3(d)]. The stable section is the upper one in consistency with the measurements.

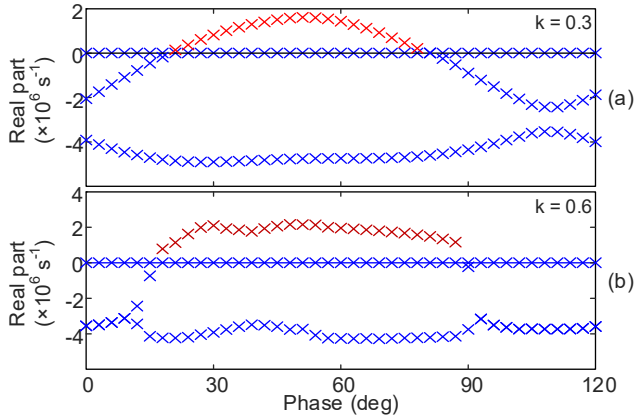


Fig. 5. Stability analysis. Real parts of the eigenvalues associated with (7) traced versus the phase shift for two k values.

The phase noise has been analyzed introducing equivalent noise sources in system (7), which provides:

$$\{j\Omega[I] - [M]\} \delta\bar{X} = \bar{I}_N \quad (8)$$

where Ω is the offset frequency from the carrier and \bar{I}_N contains the real and imaginary parts of the equivalent current noise sources (which may include upconverted flicker noise [10]). The phase noise is obtained solving for $\langle |\delta\phi_{a,1}(\Omega)|^2 \rangle$ and $\langle |\delta\phi_{b,N}(\Omega)|^2 \rangle$. For low Ω there can be inaccuracies due to the ill-conditioning of $\{j\Omega[I] - [M]\}$, often exhibited also by the conversion-matrix approach [11]. To address this problem, we have also developed a formulation of the carrier-modulation type [11]. It is obtained by replacing one of the phases in (7) with the increment in the oscillation frequency $\delta\omega$, taken as a variable, from which the (common) phase noise is calculated as: $\delta\phi = \delta\omega / (j\Omega)$. The two procedures provide the phase noise spectrum of the oscillator “b” at 3ω shown in Fig. 6(a). The calculation from $\delta\omega$ is valid at low Ω (like the HB analysis in [10]), and there is a smooth transition to (8). The spectrum is compared with the one in standalone operation. In coupled conditions, there is an improvement of about 3 dB. Note that the two oscillators are similar and based on the same devices. System (8) (relying on a linearization about each locked solution) predicts a smaller improvement from certain Ω , which depends on the system poles. The band with phase noise reduction increases for stronger coupling effects. Fig. 6(b) presents the measurements with R&S® FSWP8.

IV. CONCLUSIONS

An investigation of the global behaviour of inductively coupled oscillators at 1:N has been presented. The possibility to predict both the stability and phase noise from an outer-tier admittance system linearized about each mutually locked solution has been demonstrated for the first time to our knowledge.

ACKNOWLEDGMENT

Work supported by MCIN/AEI/10.13039/501100011033/FEDER “Una manera de hacer Europa” under research projects TEC2017-88242-C3-1-R and PID2020-116569RB-C31.

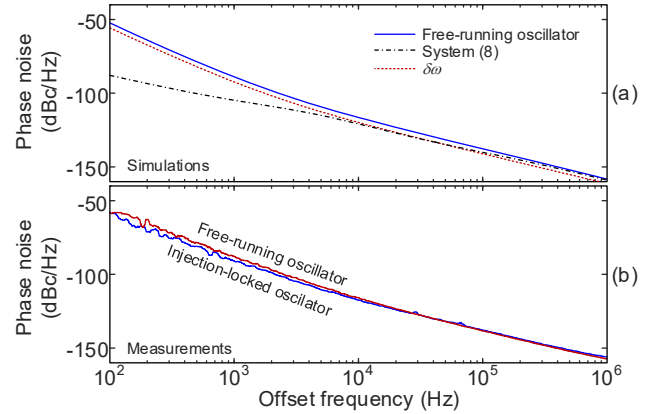


Fig. 6. Phase noise analysis at $k = 0.2$. (a) Simulated spectrum. Thicker lines indicate valid sections in each analysis. (b) Experimental.

REFERENCES

- [1] J. Rimmelpacher, R. Weigel, A. Hagelauer, V. Issakov, “A Quad-Core 60 GHz Push-Push 45 nm SOI CMOS VCO with -101.7 dBc/Hz Phase Noise at 1 MHz offset, 19% Continuous FTR and -187 dBc/Hz FoMT,” *IEEE European Solid State Circuits Conf.*, Dresden, 2018, pp. 138-141.
- [2] D. Murphy, H. Darabi, “A 27-GHz Quad-Core CMOS Oscillator With No Mode Ambiguity,” *IEEE J. Solid-State Circuits*, vol. 53, no. 11, 2018.
- [3] J. Juillard, P. Prache, N. Barniol, “Analysis of Mutually Injection-Locked Oscillators for Differential Resonant Sensing,” *IEEE Trans. Circuits Syst. I, Reg. Papers*, vol. 63, no. 7, pp. 1055-1066, July 2016.
- [4] C. Sideris, P. P. Khial, A. Hajimiri, “Design and Implementation of Reference-Free Drift-Cancelling CMOS Magnetic Sensors for Biosensing Applications,” *IEEE J. Solid-State Circuits*, vol. 53, pp. 3065-3075, 2018.
- [5] L. Chioukh, T. Djerafi, D. Deslandes, Ke Wu, “Concurrent cardiopulmonary detection using 12/24 GHz harmonic multipoint interferometer radar architecture,” *IET Microw. Ant. Propag.*, 2019, vol. 13, pp. 2396-2404.
- [6] A. Suárez, F. Ramírez, R. Melville, “Nonlinear Analysis of Oscillator Mutual Injection Locking Through Inductor Coupling,” *IEEE Trans. Microw. Theory Techn.*, vol. 69, no. 1, pp. 812-824, Jan., 2021.
- [7] A. Suárez, F. Ramírez, R. Melville, “Mutual injection locking of oscillator circuits through inductor coupling,” *IEEE MTT-S Int. Microw. Symp.*, LA, USA, 2020.
- [8] S. Sancho, A. Suárez, J. Domínguez, F. Ramírez, “Analysis of near carrier phase noise spectrum in free-running oscillators in the presence of white and colored noise sources,” *IEEE Trans. Microw. Theory Techn.*, vol. 58, no. 3, pp. 587-601, Mar., 2010.
- [9] F. Ramírez, S. Sancho, A. Suárez, “Oscillation modes in multiresonant oscillator circuits,” *IEEE Trans. Microw. Theory Techn.*, vol. 64, no. 12, pp. 4660-4675, Dec., 2016.
- [10] K. Kurokawa, “Injection locking of microwave solid-state oscillators,” in *Proceedings of the IEEE*, vol. 61, no. 10, pp. 1386-1410, Oct. 1973.
- [11] V. Rizzoli, F. Mastroi, D. Masotti, “General Noise Analysis of Nonlinear Microwave Circuits by the Piecewise Harmonic-Balance Technique,” *IEEE Trans. Microw. Theory Techn.*, vol. 42, pp. 807-819, May 1994.